ISSN (Online) 2456-1290

International Journal of Engineering Research in Mechanical and Civil Engineering (IJERMCE)

Volume 11, Issue 12, December 2024

Numerical Analysis of C18400 Copper Alloy/AlSi10Mg Aluminum Alloy Powder Beds Deposited with Bi-directional Multi-Track Selective Laser Melting

[1] Anthony J. Leslie, [2] Obeid Obeid, [3] Balaji Aresh, [4] Tony Murmu

[1][2][3][4] School of Computing, Engineering & Physical Sciences, University of the West of Scotland, United Kingdom
Email: [1] tony.leslie@uws.ac.uk, [2] obeid.obeid@uws.ac.uk, [3] balaji.aresh@uws.ac.uk, [4] tony.murmu@uws.ac.uk

Abstract*— With the increased use to Additive Manufacturing (AM) in industry, the Selective Laser Melting (SLM) method has been widely used to fabricate parts with complex geometries. Despite this, the majority of attention in industry has been paid to the use of a single material for each printed component. This material may not have superior thermal and mechanical properties at the same point in time. There is some evidence of work undertaken using two metals in AM together to create a part with enhanced properties, so called bimetallic structures. These composites such as C18400 copper alloy/AlSi10Mg aluminum alloy combine the higher conductivity from one material and the corrosion resistance and lower density of the other material in one AM part. To investigate this, 3D Finite Element Models, using ANSYS codes, have been developed to study the thermal evolution during micro-manufacturing for multi layers of C18400 and AlSi10Mg deposited on powder beds. To strengthen the metallurgical bond between layers, SLM process was simulated by altering the direction of the laser beam at 90° orientations from one layer to the next top layer. Furthermore, the laser beam moves over the layers through axial and transverse multi tracks to melt the powder. It is found that the thermal distribution about the molten pool center is symmetric when all powder particles turn into solid state. Different heat absorptivity for dissimilar layer results in a variation in the peak temperatures.

***Index Terms*— Additive manufacturing, Finite element models, Multi-material, Powder bed, Selective laser melting**

I. INTRODUCTION

Selective laser melting is one of the promising technologies in additive manufacturing because of its flexibility to manufacture complex high density metal geometries with higher degrees of flexibility and lower cost in a short process time [1]. SLM is also known as Laser-Powder Bed Fusion (L-PBF) where a high power-density laser beam interacts with powder particles to be melted layer-by-layer to form the 3D customised product.

Over the last decade, most attention had been focused on using SLM for manufacturing parts from a single powder material [2]. Although the success in developing advanced techniques to printed parts from a similar material, there has recently been a demand to form metallic parts having much better thermal and mechanical properties. Therefore, efforts have been made to develop printed products of multi-layer dissimilar materials using SLM [3]. Sun et al. proved that SLM can be used to join transition layers of Al, Cu and Al-Cu mixed powder [4]. Sing et al. investigated the interfacial characteristics formed between AlSi10Mg and C18400 using SLM [5]. They found that the interface had good metallurgical bonding. Furthermore, Wang et al. stated that Al-12Si/Al-Cu-Mg-Si bimetallic structures have a strong bond at the interface using SLM [6]. Additionally, the scanning strategy plays a crucial role in reducing residual stresses, porosity and balling effect [7]. Chen et al. found that rotating the scanning direction by 90°, so called inter-layer staggered scanning, reduces the porosity in the structure and improves the bond at the interface [8].

Due to the difficulty to observe and investigate the SLM process for micro-scale experiment, numerical simulations can implement this using the appropriate parameters, boundary conditions and software codes. Most studies reported SLM simulations have deployed either Computational Fluid Dynamics (CFD) or Finite Element Analysis (FEA). The former investigates multi-phase flow, balling occurrence and keyhole formation whilst the latter examines temperatures, molten pools and residual stresses because the thermal and mechanical boundary conditions are considered [9], [10].

In this study, 3-D FEA models have been developed to simulate laser scanning over C18400 copper alloy/AlSi10Mg aluminium alloy layers in a micro-scale powder bed to examine the predicted temperatures and molten pool dimensions. The laser beam is moving over the layer in bi-directional multi tracks using ANSYS Parametric Design Language (APDL) subroutines embedded in ANSYS Workbench software codes.

II. NUMERICAL TRANSIENT THERMAL ANALYSIS

A non-linear thermal transient model has been developed using ANSYS codes to predict thermal results along moving

ISSN (Online) 2456-1290

International Journal of Engineering Research in Mechanical and Civil Engineering (IJERMCE)

Volume 11, Issue 12, December 2024

the laser beam over the powder layers. The model is composed of a substrate on the bottom to spread 4 layers on the top. The substrate is made of stainless steel with the dimensions of 2 mm × 0.6 mm × 0.5 mm. The subsequent two layers are made of C18400 copper alloy whilst the successive top layers are made of AlSi10Mg aluminium alloy with the dimensions of 1.5 mm × 0.450 mm × 0.2 mm as shown in Fig. 1(a). To reduce the computational time, a coarser hexahedral mesh are implemented to the substrate whereas the powder layers are finely meshed with 25 µm because the thermal results are obtained when the laser beam is moving over the powder elements as shown in Fig. 1(b).

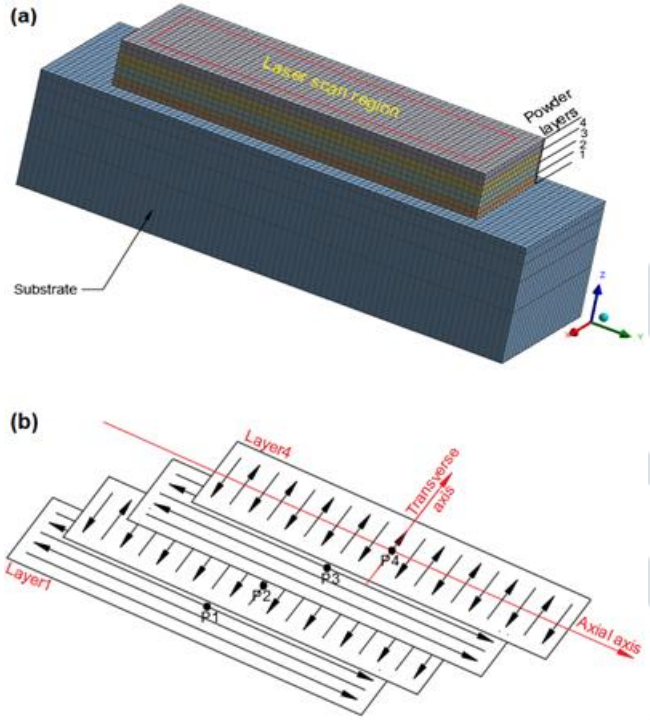

Fig. 1 (a) 3D FE model and (b) schematic sketch for scanning strategy for layers

In this simulation, some assumptions have been applied to the theoretical model to predict the thermal results:

- The powder particles are considered homogeneous with the same size 25 µm.
- The only deployed thermal boundary conditions are the conduction and convection whereas the radiation effect is ignored in this model.
- The thermal properties are temperature- dependent such as specific heat, conductivity and density.
- The density and conductivity of the powder is much lower than its respective solid material where "mpchg" command is coded as an APDL subroutine in ANSYS workbench to consider this change from powder to bulk material in the simulation.
- Element birth technique is used to deposit the layers in sequence. This requires activating the interface contact along with depositing the top subsequent layer.

During L-PBF process, the conduction is the main dominant heat loss as the laser beam interacts with the elements in layers whilst the heat loss of convection is dominant when the laser moves away during cooling time. All external surfaces exposed to the environment undergo to convective heat exchange, given by:

$$q_{conv} = -h_{conv}(T - T_a) \quad (1)$$

where q_{conv} is the convective heat loss, h_{conv} is the convective heat coefficient, T is the surface temperature and T_a is the ambient temperature which is 20°C.

The distribution of the power density, q, over the layer's surface obeys Gaussian distribution as a function of time, t, as:

$$(x, y, t) = \frac{2AP}{\pi R^2} \exp\left(-\frac{2r^2}{R^2}\right) \quad (2)$$

where A denotes to the laser energy absorptance, r denotes the radial distance from the centre of laser spot, R is the radius of the laser beam and P is the laser power.

Since the metal powder has higher porosity than its respective solid material, the density of the powder ρ_p is lower than that of the corresponding solid material ρ_{solid} based on the porosity fraction φ. In this FEA model, the porosity fraction moves from an initial powder value $\varphi_p = 0.4$ to the solid material value $\varphi_s = 0$ [11].

$$\varphi = \frac{\rho_{solid} - \rho_p}{\rho_{solid}} \quad (3)$$

As a result, the thermal conductivity, k, is associated with the temperature, T, and the porosity fraction, φ, as follows:

$$k = \begin{cases} k_p(T) & ;\ T_a \le T \le T_s \\ \frac{k_{solid}(T_m) - k_p(T_s)}{T_m - T_s}(T - T_s) + k_p(T_s) & ;\ T_s \le T \le T_m \\ k_{solid}(T) & ;\ T \ge T_m \end{cases} \quad (4)$$

$$k_p = k_{solid}(1 - \varphi)^n \quad (5)$$

where k_p and k_{solid} are the conductivities of the powder and the solid state, respectively, T_s and T_m are the sintering and melting temperatures, respectively, and n is an empirical parameter set at 4 in the presented FEA model. In this case, the layer element is assumed to initially have powder material properties. Due to the produced heat from the laser over the layer, the element temperature increases to reach T_s. Therefore, the powder phase linearly changes to be an irreversible solid state. The enthalpy, H, can be expressed as a function of temperature, T, as given below:

$$H = \int \rho c dT \quad (6)$$

where ρ and c are the material density and specific heat, respectively.

Table 1 and Table 2 summarise the thermos-physical parameters used in this simulation for C18400 and AlSi10Mg, respectively.

Table 1 Thermo-physical parameters for C18400

ISSN (Online) 2456-1290

International Journal of Engineering Research in Mechanical and Civil Engineering (IJERMCE)

Volume 11, Issue 12, December 2024

Parameters/Temp.(°C)	20	400	800	1000	1100
h_{conv} (W/m^2°C)	10				
A	0.17				
T_a (°C)	20				
T_s (°C)	800				
T_m (°C)	1000				
ρ_{solid} (kg/m^3)	8930				
k_{solid}(W/m°C)	400	376	350	343	150
c (J/kg°C)	385	427	453	460	495

Table 2 Thermo-physical parameters for AlSi10Mg

Parameters/Temp.(°C)	20	100	200	300	400
h_{conv} (W/m^2°C)	80				
A	0.09				
T_a (°C)	20				
T_s (°C)	400				
T_m (°C)	600				
ρ_{solid} (kg/m^3)	2650				
k_{solid}(W/m°C)	147	155	159	159	155
c (J/kg°C)	739	755	797	838	922

III. THERMAL RESULTS AND DISCUSSION

Fig. 2(a) and (b) shows the thermal distribution along the axial and transverse axes as the laser beam advances at P1, P2, P3 and P4 which are located at the middle of layers 1, 2, 3 and 4, respectively. For layers 1 and 3, the length of the molten pool goes along the axial direction whilst its width goes along the transverse direction. Due to the transverse laser moving over layers 2 and 4, the length of the molten pool stretches along the transverse direction whilst the width extends along the axial direction.

For Layer1, the maximum temperature is 1641°C as the laser beam advances at P1 on the third axial track in Layer1 made of C18400. The length of the molten pool, i.e. the temperature is higher than the melting temperature of C18400, 1000°C, along the axial direction is 800 µm where 575 µm is on the back end and 225 µm is on the fore part. Along the transverse direction, the temperature is higher than 1200°C at the farthest points on the width of powder bed. It is worthwhile noting that the temperatures are distributed symmetrically concerning the centre of the molten pool at P1 because the state of C18400 powder turns into solid [12].

After cooling Layer1 for 30 seconds, the laser beams resumes scanning the new deposited layer on the top of Layer1, which is Layer2. The peak temperature at P2 is 1517°C which is slightly lower than that at P1. Although both layers are made of C18400, the heat is highly accumulated in Layer1 because the conductivity of the substrate, made of stainless steel, is lower than that of C18400. Since the laser beam transversely moves in a reciprocating raster pattern, the width of the molten pool in Layer2 is extend along the axial distance as shown in Fig. 2(a). The width of the molten pool is also asymmetric at the centre P2 where it extends 475 µm and 225 µm at the back-end and front part, respectively. The length of the molten pool of Layer2 extends along the whole transverse direction, 450 µm, where the temperature distributions are almost symmetric about the centre P2 with lowest temperature at the edge of bed, ~1200°C, as shown in Fig. 2(b).

The heat absorptivity, *A*, of the laser beam plays a key role in linearly changing the magnitude of the heat density, *q*. One may note that the peak temperature at P3 on the AlSi10Mg layer reduces to 916°C because the heat absorptivity has been reduced from 0.17 for deposited C18400 layers to 0.09 for AlSi10Mg layers. The peak temperature at P4, 836°C, on Layer4 is slightly lower than that of P3 because of higher heat accumulation in C18400 Layer2. It is noteworthy that the temperature distributions along the axial and transverse directions when the laser beam advances at P3 and P4 are higher than the melting temperature of AlSi10Mg, 600°C. The thermal distribution is therefore symmetric concerning points P3 and P4 because all powder particles have changed into bulk phase [13].

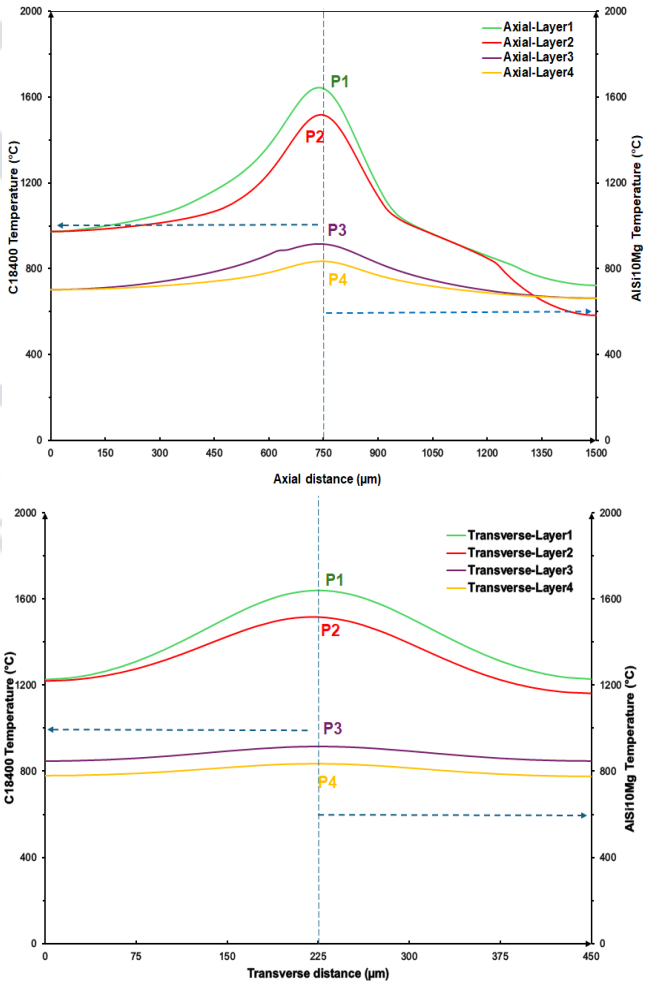

Fig. 2 Temperature map along (a) the axial axis and (b) the transverse axis as the laser passes at P1, P2, P3 and P4

IV. CONCLUSIONS

A 3-D FEA model has been implemented to simulate the

ISSN (Online) 2456-1290

International Journal of Engineering Research in Mechanical and Civil Engineering (IJERMCE)

Volume 11, Issue 12, December 2024

SLM process to manufacture one micro-scale build composed of two layers of C18400 copper alloy followed by two layers of AlSi10Mg aluminum alloy on the top. To the best of our knowledge, the FEA model for SLM with bi-directional multi-track applied in multi-layer powder bed has not been reported yet. According to the numerical thermal results, the following main conclusions can be drawn:

- Due to the change in conductivity during the transition from powder to solid phase, the thermal distribution is asymmetric concerning the melting pool center.
- The lower thermal conductivity of the dissimilar bottom layer has a significant influence in accumulation of the heat in the layer having a relatively higher one and vice versa.
- Different absorptance leads to a significant change in peak temperatures for dissimilar layers which in turn affect the molten pool dimensions.

REFERENCES

[1] C. Wei, Z. Zhang, D. Cheng, Z. Sun, M. Zhu, and L. Li, 'An overview of laser-based multiple metallic material additive manufacturing: From macro: From micro-scales', 2021. doi: 10.1088/2631-7990/abce04.

[2] J. Yang et al., 'Role of molten pool mode on formability, microstructure and mechanical properties of selective laser melted Ti-6Al-4V alloy', Mater Des, vol. 110, 2016, doi: 10.1016/j.matdes.2016.08.036.

[3] C. Wei et al., 'Understanding of process and material behaviours in additive manufacturing of Invar36/Cu10Sn multiple material components via laser-based powder bed fusion', Addit Manuf, vol. 37, p. 101683, Jan. 2021, doi: 10.1016/j.addma.2020.101683.

[4] H. Sun et al., 'Selective Laser Melting for Joining Dissimilar Materials: Investigations of Interfacial Characteristics and In Situ Alloying', Metall Mater Trans A Phys Metall Mater Sci, vol. 52, no. 4, 2021, doi: 10.1007/s11661-021-06178-9.

[5] S. L. Sing, L. P. Lam, D. Q. Zhang, Z. H. Liu, and C. K. Chua, 'Interfacial characterization of SLM parts in multi-material processing: Intermetallic phase formation between AlSi10Mg and C18400 copper alloy', Mater Charact, vol. 107, 2015, doi: 10.1016/j.matchar.2015.07.007.

[6] P. Wang et al., 'Microstructure and mechanical properties of Al-12Si and Al-3.5Cu-1.5Mg-1Si bimetal fabricated by selective laser melting', J Mater Sci Technol, vol. 36, pp. 18–26, Jan. 2020, doi: 10.1016/j.jmst.2019.03.047.

[7] B. Cheng, S. Shrestha, and K. Chou, 'Stress and deformation evaluations of scanning strategy effect in selective laser melting', Addit Manuf, vol. 12, 2016, doi: 10.1016/j.addma.2016.05.007.

[8] J. Chen, Y. Yang, C. Song, M. Zhang, S. Wu, and D. Wang, 'Interfacial microstructure and mechanical properties of 316L /CuSn10 multi-material bimetallic structure fabricated by selective laser melting', Materials Science and Engineering: A, vol. 752, 2019, doi: 10.1016/j.msea.2019.02.097.

[9] M. Zheng et al., 'A novel method for the molten pool and porosity formation modelling in selective laser melting', Int J Heat Mass Transf, vol. 140, 2019, doi: 10.1016/j.ijheatmasstransfer.2019.06.038.

[10] L. Wang, X. Jiang, Y. Zhu, X. Zhu, J. Sun, and B. Yan, 'An approach to predict the residual stress and distortion during the selective laser melting of AlSi10Mg parts', International Journal of Advanced Manufacturing Technology, vol. 97, no. 9–12, 2018, doi: 10.1007/s00170-018-2207-3.

[11] Y. Li and D. Gu, 'Parametric analysis of thermal behavior during selective laser melting additive manufacturing of aluminum alloy powder', Mater Des, vol. 63, 2014, doi: 10.1016/j.matdes.2014.07.006.

[12] J. Yin, H. Zhu, L. Ke, W. Lei, C. Dai, and D. Zuo, 'Simulation of temperature distribution in single metallic powder layer for laser micro-sintering', Comput Mater Sci, vol. 53, no. 1, 2012, doi: 10.1016/j.commatsci.2011.09.012.

[13] A. Hussein, L. Hao, C. Yan, and R. Everson, 'Finite element simulation of the temperature and stress fields in single layers built without-support in selective laser melting', Mater Des, vol. 52, 2013, doi: 10.1016/j.matdes.2013.05.070.